International Journal for Modern Trends in Science and Technology
Volume 12, Issue 04, pages 648-660.
ISSN: 2455-3778 online
Available online at: http://www.ijmtst.com/vol12issue04.html
DOI: https://doi.org/10.5281/zenodo.19536613

Grid-Independent UPQC Operation Using Solar PV, Battery Storage, and EV for Enhanced Power Quality under Voltage Disturbances

B.Sekhar, Y.Venkata Saraswathi, B.Pavan Kumar, D. Dhanush, G.Santosh Sagar

Department of Electrical and Electronics Engineering, Vasireddy Venkatadri Institute of Technology, Pedakakani, Namburu, Guntur, India.

To Cite this Article
B.Sekhar, Y.Venkata Saraswathi, B.Pavan Kumar, D. Dhanush & G.Santosh Sagar (2026). Grid-Independent UPQC Operation Using Solar PV, Battery Storage, and EV for Enhanced Power Quality under Voltage Disturbances. International Journal for Modern Trends in Science and Technology, 12(04), 648-660. https://doi.org/10.5281/zenodo.19536613

Article Info
Received: 16 March 2026; Revised: 06 April 2026; Accepted: 10 April 2026.

KEYWORDS

Unified Power Quality Conditioner (UPQC), solar photovoltaic (PV), electric vehicle (EV), battery energy storage system (BESS), voltage sag and swell compensation, harmonic mitigation, reactive power compensation, grid-independent operation, microgrid, power quality improvement, bidirectional power flow.

ABSTRACT

This paper presents a grid-independent Unified Power Quality Conditioner (UPQC) integrated with solar photovoltaic (PV), battery storage, and an electric vehicle (EV) for enhancing power quality and ensuring reliable power supply under voltage disturbances. The proposed system effectively mitigates common power quality issues such as voltage sag, swell, harmonics, and reactive power imbalance. The UPQC employs both series and shunt converters, where the series converter compensates voltage disturbances to maintain a stable load voltage, and the shunt converter eliminates current harmonics, improves power factor, and regulates the DC-link voltage. The integration of PV serves as a primary renewable energy source, while the battery and EV provide additional energy support through bidirectional power flow. During grid disturbances or outages, the system operates in islanded mode, where PV, battery, and EV collectively supply the load, ensuring uninterrupted operation. The EV further enhances system flexibility by acting as a mobile energy storage unit capable of both charging and discharging. An advanced control strategy enables seamless coordination between the UPQC and distributed energy sources, ensuring effective compensation and stable operation under dynamic conditions. Simulation results validate that the proposed system successfully corrects voltage sag and swell, reduces harmonic distortion, and significantly improves overall power quality at the point of common coupling. The system offers a reliable, flexible, and sustainable solution for modern microgrid and EV-integrated applications.

1. INTRODUCTION

The global transition toward sustainable and clean energy systems has accelerated significantly in recent years due to rising environmental concerns, depletion of fossil fuels, and stringent emission regulations. Renewable energy sources, particularly solar photovoltaic (PV) systems, have emerged as a key solution for reducing carbon emissions and ensuring energy sustainability [1], [2]. The integration of PV systems into microgrids and distribution networks has gained widespread attention due to their modularity, scalability, and decreasing installation costs [3]. However, the intermittent and variable nature of solar energy introduces challenges in maintaining system stability, reliability, and power quality [4], [5]. Simultaneously, the rapid adoption of electric vehicles (EVs) is reshaping the transportation and energy sectors. EVs not only serve as eco-friendly transportation alternatives but also act as distributed energy storage units when integrated with power systems [6], [7]. Through bidirectional power flow capability, commonly referred to as Vehicle-to-Grid (V2G) technology, EVs can support grid operations by supplying stored energy during peak demand and absorbing excess energy during off-peak periods [8], [9]. This dual functionality enhances grid flexibility and enables efficient energy management in modern smart grids and microgrids [10]. Despite these advantages, the increased penetration of PV systems, EV charging stations, and power electronic converters introduces significant power quality issues in the distribution network. Problems such as voltage sag, voltage swell, harmonics, flicker, and reactive power imbalance are becoming more prevalent due to the widespread use of non-linear loads and switching devices [11]–[13]. These disturbances can degrade system performance, reduce equipment lifespan, and adversely affect sensitive loads such as industrial automation systems, medical equipment, and communication devices [14], [15]. Therefore, maintaining high power quality has become a critical requirement in modern power systems. To address these challenges, various custom power devices have been developed, among which the Unified Power Quality Conditioner (UPQC) is one of the most effective solutions. The UPQC integrates both series and shunt active power filters to simultaneously compensate for voltage and current-related disturbances [16], [17]. The series converter injects a compensating voltage to mitigate voltage sag, swell, and unbalance, thereby ensuring a stable and distortion-free load voltage. Meanwhile, the shunt converter eliminates current harmonics, compensates reactive power, and regulates the DC-link voltage [18], [19]. This dual functionality makes the UPQC highly suitable for improving overall power quality at the point of common coupling (PCC). Conventional UPQC systems, however, are typically dependent on the utility grid for their operation. During grid disturbances, faults, or outages, these systems may fail to provide continuous compensation and reliable power supply to critical loads [20]. To overcome this limitation, recent research has focused on the development of grid-independent or islanded UPQC systems, which utilize local energy sources such as PV and battery energy storage systems (BESS) [21], [22]. In such configurations, the UPQC not only performs power quality compensation but also ensures uninterrupted power supply by operating independently of the grid during abnormal conditions. The integration of battery energy storage systems plays a crucial role in enhancing the reliability and performance of grid-independent UPQC systems. Batteries provide energy buffering, support DC-link voltage stabilization, and enable smooth transitions between different operating modes [23]. However, relying solely on battery storage may not be sufficient for long-duration backup or dynamic load variations. In this context, the inclusion of EVs as additional energy storage resources offers significant advantages. EVs can operate in both charging (G2V) and discharging (V2G) modes, thereby contributing to load support, peak shaving, and energy balancing within the microgrid [24]. The combined integration of PV, battery storage, and EV within a UPQC-based microgrid creates a highly flexible and resilient energy system. However, this integration also introduces challenges related to system coordination, control complexity, and energy management. The system must ensure seamless mode transitions between grid-connected and islanded operation, efficient power sharing among multiple sources, and stable DC-link voltage under dynamic conditions [25]. Furthermore, the control strategy must effectively handle power quality

compensation while maintaining system stability and minimizing harmonic distortion. In this paper, a grid-independent UPQC system integrated with solar PV, battery storage, and EV is proposed to enhance power quality and ensure reliable operation under voltage disturbances. The proposed system is capable of mitigating voltage sag, swell, harmonics, and reactive power issues while simultaneously supporting load demand during grid outages. The EV is utilized as a mobile energy storage unit, providing additional flexibility through bidirectional power flow. An advanced control strategy based on synchronous reference frame (SRF) theory is implemented to achieve precise compensation, efficient energy management, and stable system performance. The effectiveness of the proposed system is validated through detailed simulations carried out in MATLAB/Simulink. The results demonstrate significant improvement in power quality, reduced total harmonic distortion (THD), stable load voltage under disturbances, and efficient coordination among PV, battery, EV, and UPQC components. The proposed approach provides a robust, sustainable, and intelligent solution for next-generation smart microgrids and EV-integrated energy systems.

II. SYSTEM CONFIGURATION

The system configuration illustrated in Fig. 1 represents an integrated power electronic interface combining grid supply, renewable energy sources, energy storage, and electric vehicle (EV) charging within a unified control structure. The grid is modeled as a three-phase voltage source with internal impedance, supplying power to the network. A series converter is connected through coupling inductors to inject a controllable voltage into the transmission line, thereby regulating power flow and mitigating disturbances. In conjunction with this, a shunt converter is connected in parallel with the grid, forming a configuration analogous to a Unified Power Flow Controller (UPFC). The shunt converter is responsible for maintaining the DC-link voltage and providing reactive power compensation to support voltage stability. Both converters share a common DC-link capacitor, which facilitates bidirectional power exchange between the AC and DC subsystems. On the DC side, multiple distributed energy resources and loads are interfaced through appropriate DC–DC converters. A solar photovoltaic (PV) system is connected via a DC–DC boost converter to regulate and elevate its output voltage to the DC-link level. In addition, a battery energy storage system (BESS) is integrated through a bidirectional DC–DC buck–boost converter, enabling both charging and discharging operations for energy management and system support. Furthermore, an EV charging unit is supplied through a dedicated DC–DC boost converter, which ensures controlled voltage and current delivery to the vehicle battery. The coordinated control of these converters allows efficient power flow management among the grid, renewable sources, storage units, and loads. Overall, the proposed system enhances power quality, ensures DC-link voltage stability, and facilitates flexible integration of renewable energy and EV charging infrastructure in modern power systems.

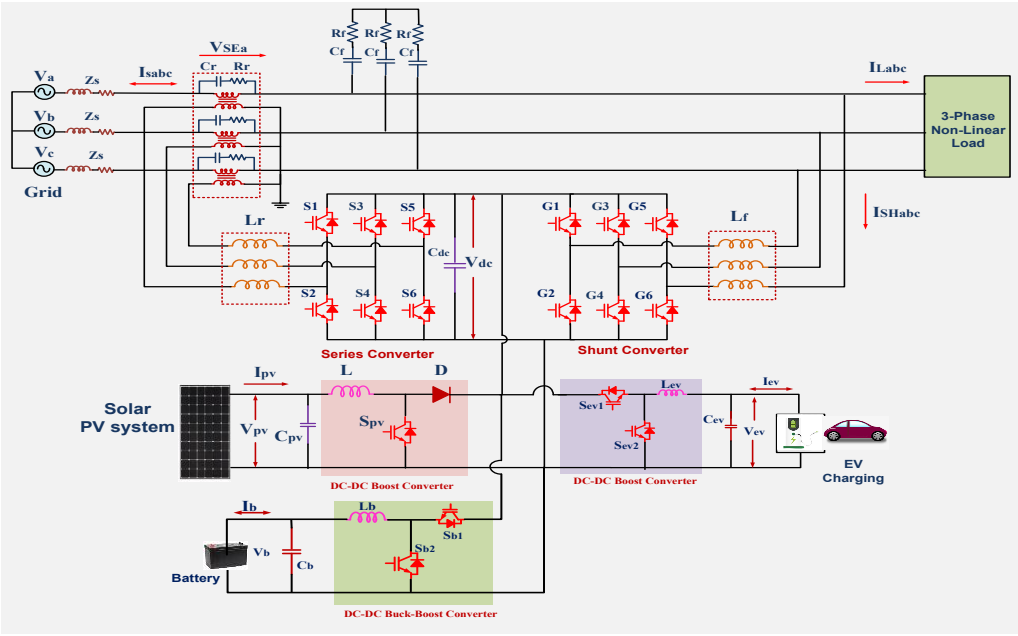

Fig. 1. Unified Power Flow Controller (UPFC)-Based Grid Interface with DC Microgrid and EV Load.

III. MODELING AND DESIGNING OF PROPOSED SYSTEM CONFIGURATION

A. Solar PV Modeling and Designing with Boost Converter and P&O MPPT Algorithm

1. Solar PV System Modeling

A Photovoltaic (PV) system converts solar energy into electrical power using photovoltaic cells. The output power of a PV module depends on factors such as solar irradiance, temperature, and load conditions. The general mathematical model of a solar PV module is derived from the single-diode equivalent circuit and is expressed as:

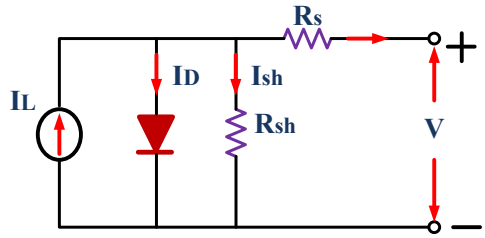

Fig. 2 equivalent model of PV solar.

$$I = I_{ph} - I_o\left(e^{\frac{q(V+IR_S)}{nKT}} - 1\right) - \frac{V+IR_S}{R_{sh}} \quad (1)$$

Where:

- Iph = Photogenerated current (dependent on solar irradiance and temperature)
- Io = Reverse saturation current
- q = Electron charge (1.6×10^{-19} C)
- V = PV module output voltage
- I = PV module output current
- Rs = Series resistance of the PV cell
- Rsh = Shunt resistance of the PV cell
- n = Ideality factor of the diode
- K = Boltzmann's constant (1.38×10^{-23} J/K)
- T = Temperature in Kelvin

B. Solar PV Boost Converter with P&O MPPT Algorithm

A solar PV boost converter with a Perturb and Observe (P&O) MPPT algorithm is designed to maximize power extraction from a photovoltaic (PV) panel while ensuring the output voltage is suitable for the connected load or battery as shown in Fig.3. The PV panel generates DC electricity, but its output varies with irradiance and temperature, requiring an MPPT controller to operate at the Maximum Power Point (MPP). A boost converter, consisting of an inductor, MOSFET switch, diode, and capacitor, is used to step up the PV voltage. When the MOSFET switch is ON, the inductor stores energy from the PV panel, and when the MOSFET is OFF, the inductor releases energy to the output, thereby increasing the voltage.

The output voltage (Vo) is controlled by adjusting the duty cycle (D) using the relation

$$V_0 = V_{PV} / (1 - D) \quad (2)$$

The P&O MPPT algorithm works by continuously perturbing the PV voltage and observing the resulting power change. It first measures the PV voltage (Vpv) and current (Ipv), then calculates the power (Ppv). If a small increase in voltage leads to an increase in power, the algorithm continues perturbing in the same direction; otherwise, it reverses the perturbation to reach the MPP. This iterative process ensures that the PV panel operates at its highest efficiency. The combination of the boost converter and P&O MPPT controller effectively regulates the PV output, improving energy harvesting efficiency and providing a stable power supply for various applications.

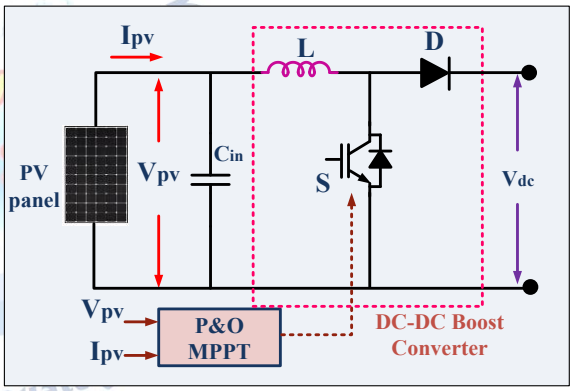

Fig. 3 solar PV P&O MPPT DC-DC boost converter

C. Perturb and Observe (P&O) MPPT Algorithm

The Perturb and Observe (P&O) Maximum Power Point Tracking (MPPT) algorithm is one of the most widely used techniques for optimizing the power output from a solar photovoltaic (PV) system. The power generated by a PV panel depends on environmental conditions such as solar irradiance and temperature, making it necessary to continuously track the Maximum Power Point (MPP) for efficient operation as shown in Fig.4. The P&O algorithm operates by making small perturbations (incremental changes) to the PV voltage (Vpv) and observing the resulting changes in power (Ppv). Based on this observation, the algorithm decides whether to continue perturbing in the same direction or to reverse the perturbation to ensure that the system remains near the MPP. The working can be summarized as follows:

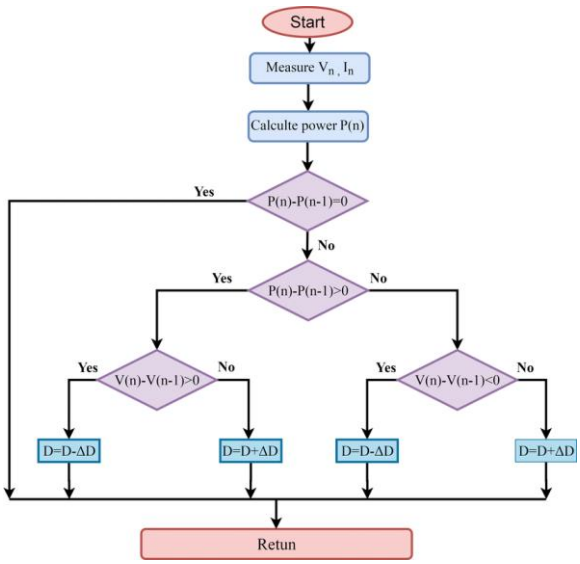

Fig. 4 flow chart of P&O MPPT algorithm

1. Measure the PV voltage (Vpv) and current (Ipv), then compute the power:

$$P_{Pv} = V_{Pv} \times I_{Pv} \quad (3)$$

2. Compare the new power value with the previous power value (Ppv(n) and Ppv(n−1)):

- If Ppv(n)>Ppv(n−1), it means the system is moving towards the MPP, so the voltage perturbation is maintained in the same direction.
- If Ppv(n)<Ppv(n−1), it indicates that the system has moved away from the MPP, so the voltage perturbation direction is reversed.

The process continues iteratively to keep the system at or near the maximum power point. The decision-making process of the P&O algorithm is expressed as:

$$if\ dP_{Pv}/dV_{pv} > 0 \rightarrow increase\ v_{pv} \quad (4)$$

$$if\ dP_{Pv}/dV_{pv} < 0 \rightarrow decrease\ v_{pv} \quad (5)$$

Where

$$dP_{Pv} = P_{pv}(n) - p_{pv(n-1)} \quad (6)$$

$$dV_{Pv} = V_{pV}(n) - V_{pv(n-1)} \quad (7)$$

The duty cycle (D) of the boost converter is adjusted accordingly to ensure the operating point moves toward the MPP. The duty cycle is updated as:

$$D(n) = D(n-1) \pm \Delta D \quad (8)$$

Where ΔD is the perturbation step size.

D. Modeling and Designing of a Bidirectional Buck-Boost Converter

1. Introduction and System Overview

The combined strengths of lithium-ion batteries enable the development of efficient energy storage systems that leverage their high energy density and reliability, as shown in Fig. 5. The DC bus and these storage units can be effectively managed using a bidirectional buck–boost converter. This converter facilitates power flow in both directions, allowing energy transfer from the DC bus to the battery during charging and from the battery to the load during discharging. Its capability to perform both step-down (buck) and step-up (boost) operations ensures proper voltage regulation under varying operating conditions. The converter plays a crucial role in maintaining stable DC bus voltage and controlling battery charging and discharging processes, thereby enhancing overall system performance and efficiency.

2. Operating Modes

The converter operates in two primary modes:

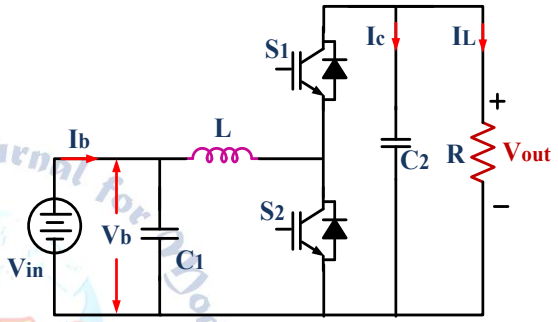

Fig.5 circuit diagram of DC-DC bidirectional buck boost converter

- **Buck Mode (Step-Down):** When the voltage on the DC bus is lower than the battery voltage (or supercapacitor voltage), the converter operates in buck mode to step down the voltage. This is typically used when discharging energy from the storage system to the bus or load.
- **Boost Mode (Step-Up):** When the voltage on the DC bus is higher than the storage voltage, the converter operates in boost mode to step up the voltage. This mode is used when charging the storage elements from the DC bus.

A single converter can operate in either mode by adjusting the duty cycle of its switching devices. In bidirectional operation, the power electronics (usually using MOSFETs or IGBTs) are arranged in an H-bridge or similar topology to allow current flow in both directions.

$$V_{out} = D \cdot V_{in} \quad (5)$$

Where: Vin is the input voltage (from the battery or DC bus), Vout is the regulated output voltage (to the load or storage device), D is the duty cycle, with 0<D<1.

3. Boost Mode (Step-Up Operation)

In boost mode, the converter increases the input voltage to a higher output voltage. The output voltage is expressed as:

$$V_{out} = \frac{V_{in}}{(1-D)} \quad (6)$$

Where: Vin is the lower voltage from the storage device or DC bus, Vout is the higher regulated voltage, D is the duty cycle, with 0<D<1.

4. Inductor and Capacitor Design

For both modes, an inductor L and output capacitor C are essential for smoothing the current and voltage ripples.

Inductor Design

To ensure continuous conduction mode (CCM) and limit the inductor current ripple (ΔIL), the inductor value can be estimated by:

$$L = \frac{(V_{in} - V_{out}) \cdot D}{f_s - \Delta I_L} \quad (7)$$

$$L = \frac{V_{in} \cdot D}{f_s - \Delta I_L} \quad (8)$$

Where: f_s is the switching frequency, ΔI_L is the desired peak-to-peak inductor current ripple.

Capacitor Design

The output capacitor C smooths the voltage ripple (ΔV_{out}) at the output and is given by:

$$C = \frac{I_{out} \cdot D}{f_s - \Delta V_{out}} \quad (9)$$

Where: I_{out} is the load or charging current, ΔV_{out} is the acceptable output voltage ripple.

E. Modeling and Designing of Lithium-Ion Battery.

In modern power systems, Hybrid Energy Storage Systems (HESS) integrates multiple energy storage devices to enhance overall energy and power performance. Lithium-ion batteries, owing to their high energy density and efficiency, are widely utilized for sustained energy supply in such systems. The incorporation of multiple battery units facilitates improved operational flexibility and effective load management under varying conditions. This configuration enables enhanced load balancing, mitigates stress on individual battery units, and extends overall battery lifespan. Furthermore, it improves system responsiveness and reliability, making it highly suitable for applications such as electric vehicle (EV) charging, renewable energy integration, and microgrid operations.

a. Lithium-Ion Battery Modeling

The lithium-ion battery used in the proposed system is modeled using a nonlinear dynamic equation that captures both charging and discharging characteristics. The battery terminal voltage is expressed as:

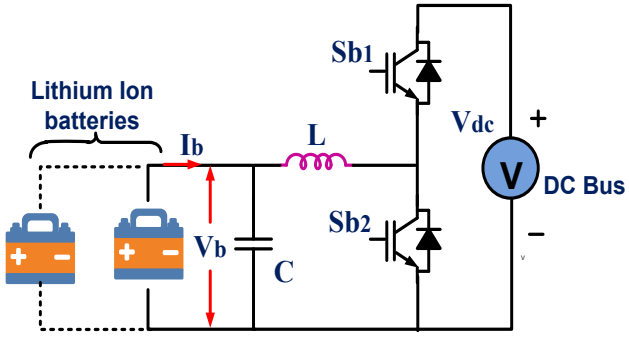

Fig.6 principle operation bidirectional dc-dc buck boost converter

$$E_B = E_0 - \frac{KQI_B}{Q - \int I_B \, dt} - k\frac{Q}{Q - \int I_B \, dt} \int I_B dt + A \exp(-B \int I_B \, dt) \quad (10)$$

where E_B represents the battery terminal voltage, E_0 is the constant open-circuit voltage, K denotes the polarization constant (V/Ah), Q is the maximum battery capacity (Ah), and IB is the battery current. The term $\int I_B \, dt)$ represents the extracted capacity over time. The exponential term $\exp(-B \int I_B \, dt)$ models the voltage behavior in the exponential region of the battery discharge curve, where A and B are empirical constants. This model effectively captures the nonlinear voltage characteristics of lithium-ion batteries under varying load conditions. It accounts for polarization effects, capacity variation, and transient response during charging and discharging. The State of Charge (SoC) of the battery is estimated based on the integration of battery current, enabling accurate monitoring and control of energy storage units. The developed battery model is implemented for each BESS unit in the system, allowing decentralized control and SoC balancing across multiple batteries to enhance system reliability and lifespan.

F. Double-Loop Controller for EV Charging System

A double-loop control system is used as part of the control strategy for electric vehicle (EV) charging in order to guarantee safe, efficient, and reliable charging. The inner current loop controls the current going into the batteries, while the outside voltage loop keeps the DC bus voltage constant. To enhance dynamic performance and decrease steady-state error, a Proportional-Integral (PI) controller is used in both loops.

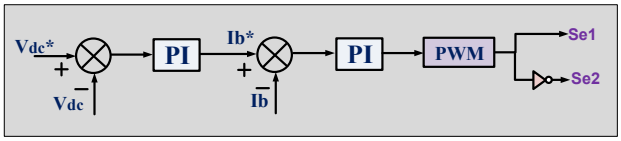

Fig. 7 double loop battery charging controller

1. Outer Voltage Loop: DC Bus Voltage Control

The outer voltage loop ensures the DC bus voltage (V_{dc}) remains stable and within the desired range. Since variations in EV charging loads and grid fluctuations affect the DC bus voltage, this loop provides a reference current (I_{ev}^{*}) for the inner current loop.

Error Signal Calculation:

$$e_v(t) = V_{dc}^{*} - V_{dc} \quad (11)$$

PI Controller Output (Reference EV Charging Current I_{ev}^{*}

$$I_{ev}^{*}(t) = K_{PV} e_v(t) + k_{iv} \int e_v(t)\, dt \quad (12)$$

Where: I_{ev}^{*}= Reference charging current for the inner loop, K_{PV} = Proportional gain of voltage controller, k_{iv}= Integral gain of voltage controller

This reference current is then passed to the inner current loop for precise battery charging control.

2. Inner Current Loop: Battery Current Control

To avoid overcharging and battery deterioration, the electric vehicle's inner current loop controls the charging current. Here, the PI controller determines the DC-DC converter's duty cycle, whether it's a buck or a boost.

Error Signal Calculation:

$$e_i(t) = I_{ev}^{*} - I_{ev} \quad (13)$$

PI Controller Output (Duty Cycle Control)

$$D(t) = K_{Pi} e_i(t) + k_{ii} \int e_i(t)\, dt \quad (14)$$

Where: D = Duty cycle of the DC-DC converter, Kpi= Proportional gain of current controller, Kii= Integral gain of current controller

This duty cycle (D) is applied to the DC-DC converter, adjusting the output voltage and current to regulate battery charging.

IV. CONTROL OF UPQC

An innovative approach to controlling power quality while harnessing renewable energy sources is the UPQC-PV-WE-ESS system. It improves grid dependability and system efficiency by reducing voltage problems such as sags, swells, harmonics, and flickers. This setup makes the most of the UPQC's capabilities by combining its shunt and series compensator features. Shunt compensators dynamically change compensation currents, which helps alleviate power quality concerns including reactive power and load current harmonics. By converting wind energy into usable electricity and collecting sunlight, it also makes it easier to incorporate renewable energy sources. By injecting suitable voltages in phase with the grid voltage, the series compensator safeguards against poor grid power quality and guarantees a steady, high-quality power supply to the load. Additionally, the system incorporates energy storage, which helps with backup power during grid outages, improves grid dependability, and adds to the overall resilience of the energy system. Figure 8 shows that the UPQC-PV-WE-ESS system compensates for the load current using the Selective Harmonic Reduction Factor (SRF) method, and that it does this by using a proportional-integral (PI) controller to regulate the DC-link voltage at the produced reference. To achieve exact grid synchronization, phase-locked loop (PLL) data is used to transform load currents into the dq0 domain. We use a moving average filter (MAF) to keep the system responsive while minimizing effect on dynamic performance. In conclusion, the UPQC-PV-WE-ESS system does a good job of managing power quality concerns, incorporating renewable energy sources, and building a more robust and sustainable energy future.

A. Control of Shunt Compensator

The shunt converter of the Unified Power Quality Conditioner (UPQC) is responsible for compensating current harmonics, reactive power, and regulating the DC-link voltage at the point of common coupling (PCC). It operates as a controlled current source inverter and ensures that the source currents remain sinusoidal, balanced, and in phase with the supply voltage even under non-linear load conditions. The control strategy is based on the synchronous reference frame (SRF) theory, which enables decoupled control of active and reactive current components.

Initially, the DC-link voltage Vdc is measured and compared with the reference value Vdcref. The resulting error signal is expressed as:

$$e(t) = V_{dc}^{ref} - V_{dc} \quad (15)$$

This error is processed through a proportional-integral This error is processed through a proportional-integral (PI) controller to generate the reference direct-axis current id∗, which governs the active power exchange:

$$i_d^* = K_p e(t) + K_i \int e(t)dt \quad (16)$$

where Kp and Ki are the proportional and integral gains, respectively.

The three-phase load currents (ia,ib,ic) are transformed into the synchronous rotating reference frame using Park's transformation. The transformation angle θ is obtained from a phase-locked loop (PLL) synchronized with the grid voltage. The transformation is given by:

$$\begin{bmatrix} i_d \\ i_q \\ i_0 \end{bmatrix} = \frac{2}{3} \begin{bmatrix} \cos\theta & \cos\left(\theta - \frac{2\pi}{3}\right) & \cos\left(\theta + \frac{2\pi}{3}\right) \\ -\sin\theta & -\sin\left(\theta - \frac{2\pi}{3}\right) & -\sin\theta\left(\theta + \frac{2\pi}{3}\right) \\ \frac{1}{2} & \frac{1}{2} & \frac{1}{2} \end{bmatrix} \begin{bmatrix} i_a \\ i_b \\ i_c \end{bmatrix} \quad (17)$$

In the dq frame, the fundamental components appear as DC quantities, while harmonic components become oscillatory signals. To extract the fundamental components, low-pass filters (LPFs) are used:

$$i_d^{fund} = LPF(i_d) \quad (18)$$

$$i_q^{fund} = LPF(i_q) \quad (19)$$

The harmonic components can be obtained as:

$$i_d^{harm} = i_d - i_d^{fund} \quad (20)$$

$$i_q^{harm} = i_q - i_q^{fund} \quad (21)$$

For unity power factor operation, the reference quadrature-axis current is set to:

$$i_q^* = 0 \quad (22)$$

The reference current components are then defined as:

$$i_d^{ref} = i_d^* - i_d^{fund} \quad (23)$$

$$i_q^{ref} = -i_q^{fund} \quad (24)$$

These compensating components ensure that harmonic and reactive currents are eliminated.

The reference dq currents are transformed back into the three-phase stationary frame using inverse Park transformation:

$$\begin{bmatrix} i_a^* \\ i_b^* \\ i_c^* \end{bmatrix} = \begin{bmatrix} \cos\theta & -\sin\theta & 1 \\ \cos\left(\theta - \frac{2\pi}{3}\right) & -\sin\left(\theta - \frac{2\pi}{3}\right) & 1 \\ \cos\left(\theta + \frac{2\pi}{3}\right) & -\sin\theta\left(\theta + \frac{2\pi}{3}\right) & 1 \end{bmatrix} \begin{bmatrix} i_d^{ref} \\ i_q^{ref} \\ i_0 \end{bmatrix} \quad (25)$$

The generated reference currents (ia∗,ib∗,ic∗) are compared with the actual converter currents (ia,ib,ic), and the resulting error is fed into a hysteresis current controller. The current error is defined as:

$$i_{error} = i_{abc}^* - i_{abc} \quad (25)$$

The hysteresis controller generates switching signals based on a predefined band hhh:

- If ierror>+hi_{error} > +hierror>+h, upper switch OFF, lower switch ON
- If ierror<−hi_{error} < -hierror<−h, upper switch ON, lower switch OFF

This control ensures fast dynamic response and accurate current tracking.

Finally, the hysteresis controller produces six PWM gate signals corresponding to the six switches of the three-phase shunt converter. These signals enable the converter to perform multiple functions simultaneously, including DC-link voltage regulation, harmonic compensation, and reactive power support. As a result, the UPQC shunt converter significantly improves power quality by reducing total harmonic distortion (THD), maintaining unity power factor, and ensuring stable operation under dynamic load conditions.

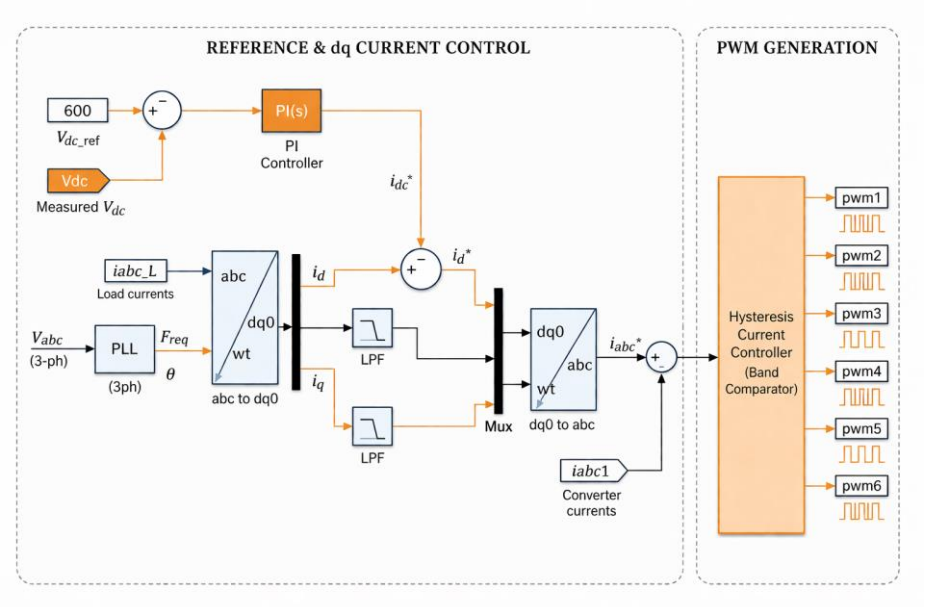

Fig. 8. Control Structure of Shunt Compensator

B. Control of Series Compensator

Fig. 9 shows that a control method called a series compensator may reduce the amount of voltage injection required by bringing it into phase with the grid voltage. A phase-locked loop (PLL) is used to provide the reference load voltage after generating the fundamental component of the Point of Common Coupling (PCC) voltage. The load reference voltage's peak value is corresponding to the d-axis component, whereas the q-axis component is zero. To get the series compensator reference voltage, subtract the PCC voltage from the load reference voltage. You may find the real series compensator voltages by comparing the load voltage with the PCC voltage. In order to generate accurate reference signals, proportional-integral (PI) controllers receive this disparity. After that, the signals are converted to the abc domain and fed into the series compensator's appropriate gating circuits using pulse width modulation (PWM) voltage controllers. Aligning the series compensator with the grid voltage and enhancing its performance, this full control scheme guarantees it operates appropriately. It makes the power better and the grid more stable.

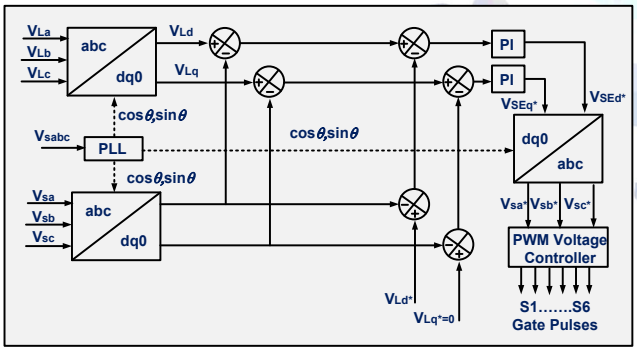

Fig. 9 Control Structure of Series Compensator

V. RESULTS AND DISCUSSION

A. System Response Under Varying Operating Conditions

The simulation results show that the grid voltage remains stable and sinusoidal over the entire duration from 0 to 1 s, with peak values between 350 V and −350 V, indicating a balanced three-phase supply without any disturbance. In contrast, the grid current exhibits dynamic changes over time. At the initial stage (t = 0 to 0.2 s), the current reaches a high magnitude of 45 A, which suggests a transient or startup condition. After t ≈ 0.2 s, the current magnitude decreases and stabilizes around ±20–25 A, indicating a transition to a lower power operating condition. From t ≈ 0.4 s to 0.6 s, the current further reduces and appears more controlled, remaining roughly within 10–15 A. A significant change occurs at t ≈ 0.6 s, where the current waveform shifts downward into the negative region, reaching approximately −20 A to −30 A, indicating a reversal in power flow or a change in operating mode (such as inverter absorption or load variation). This negative current persists until about t ≈ 0.75 s, after which the current starts increasing again. At t ≈ 0.8 s, the current transitions back to positive values around 20 A, and finally, by t ≈ 0.9 to 1 s, it rises further to approximately 40 A, indicating a higher power injection into the grid. Additionally, the dc-link or control current (Iev) plot shows step-like behavior corresponding to these transitions. Initially (t = 0 s), the current starts near +50 A and quickly drops to around 0 A within 0.05 s, suggesting a fast transient response. It remains close to zero until t ≈ 0.6 s, where it sharply decreases to approximately −30 A, followed by a further dip to about −40 A at t ≈ 0.7 s. Subsequently, the current rises to around 20 A at t ≈ 0.8 s and finally reaches approximately 40–45 A by t ≈ 0.9–1 s. Overall, the results demonstrate that while the grid voltage remains unaffected and stable, the current dynamically adjusts in discrete steps, clearly reflecting changes in load demand or control strategy. The system shows good transient response and stability, with smooth transitions between operating regions and no visible oscillations or instability.

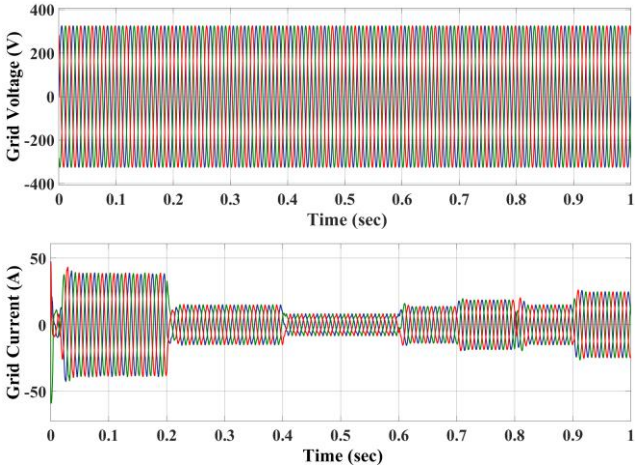

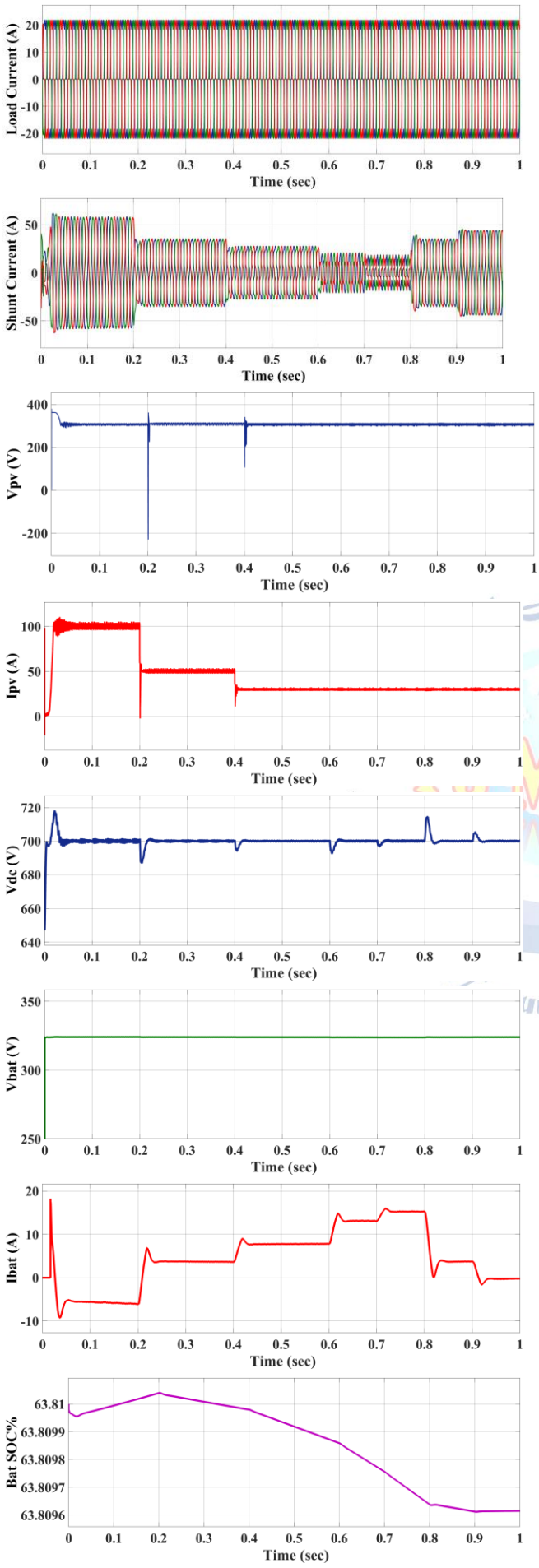

Simulation results of proposed system varying operating conditions

B. Voltage Sag and Swell Compensation Analysis

From the presented waveforms, the grid voltage clearly shows both sag and swell conditions over the time interval 0 to 1 s. Initially, from t = 0 to 0.2 s, the grid voltage is at its nominal level with peak values around 300 V. At t ≈ 0.2 s, a voltage sag occurs, where the amplitude of the grid voltage reduces significantly to approximately 150–180 V, indicating nearly a 40–50% drop in voltage magnitude. This sag condition persists until about t ≈ 0.4 s. To compensate for this sag, the series injected voltage becomes active during the same interval (0.2 s to 0.4 s). The injected voltage waveform rises from zero to approximately 120–150 V, which is in phase with the grid voltage, thereby boosting the reduced supply voltage. As a result, the load voltage remains almost unaffected and continues to stay at its nominal value of approximately 300 V, demonstrating effective sag compensation. Between t ≈ 0.4 s and 0.6 s, the grid voltage returns to its normal level (300 V), and the series injected voltage drops back to zero, indicating no compensation is required. The load voltage remains stable during this period. At t ≈ 0.6 s, a voltage swell condition occurs, where the grid voltage increases beyond its nominal value to approximately 400–450 V. This represents a significant overvoltage condition. In response, the series injected voltage is again activated, but this time it injects a voltage in opposition (negative polarity relative to the grid), with magnitude around 100–120 V, effectively

reducing the excess voltage. Due to this compensation, the load voltage remains regulated at around 300 V, even during the swell condition (0.6 s to 0.8 s). After t ≈ 0.8 s, the grid voltage returns to normal, the injected voltage becomes zero again, and the load voltage continues steady operation. Overall, the results confirm that the system successfully mitigates both voltage sag (0.2–0.4 s) and voltage swell (0.6–0.8 s) conditions. The series compensation maintains a constant load voltage (300 V) despite significant variations in the grid voltage, demonstrating effective dynamic voltage restoration performance.

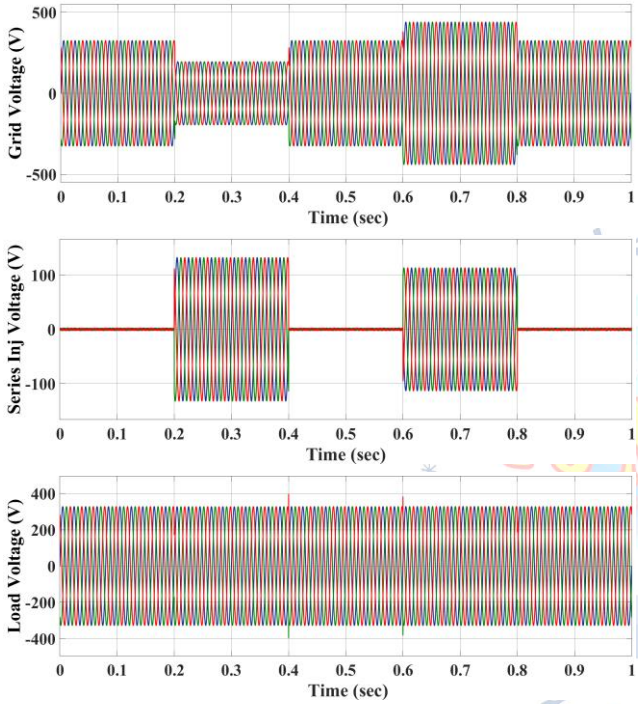

Simulation analysis of Voltage Sag and Swell Performance

VI. Conclusion

This paper presented a grid-independent Unified Power Quality Conditioner (UPQC) integrated with solar PV, battery storage, and an electric vehicle (EV) to enhance power quality and ensure reliable power supply under voltage disturbances. The proposed system effectively addressed major power quality issues, including voltage sag, swell, harmonics, and reactive power imbalance. The simulation results demonstrated that the series converter successfully maintained a constant load voltage during sag and swell conditions, while the shunt converter effectively reduced current harmonics, improved power factor, and regulated the DC-link voltage. The integration of solar PV as a primary energy source, along with battery storage and EV support, enabled continuous and stable power delivery, even during grid disturbances and islanded operation. The bidirectional capability of the battery and EV provided additional flexibility in power management, ensuring efficient energy utilization and uninterrupted load supply. Furthermore, the coordinated control strategy ensured smooth operation and fast dynamic response under varying operating conditions. Overall, the proposed system proved to be a reliable, flexible, and sustainable solution for modern power systems, particularly in microgrid and EV-integrated applications. It significantly enhances power quality and system resilience, making it suitable for future smart grid implementations. Future work may focus on real-time hardware implementation and optimization of control strategies for improved efficiency and scalability.

Conflict of interest statement

Authors declare that they do not have any conflict of interest.

References

[1] K. Padmanathan, U. Govindarajan, V. K. Ramachandaramurthy, A. Rajagopalan, N. Pachaivannan, U. Sowmmiya, S. Padmanaban, J. B. Holm-Nielsen, S. Xavier, and S. K. Periasamy, ``A sociocultural study on solar photovoltaic energy system in India: Strati_cation and policy implication,'' J. Cleaner Prod., vol. 216, pp. 461_481, Apr. 2019.

[2] R. M. Elavarasan, G. Sha_ullah, S. Padmanaban, N. M. Kumar, A. Annam, A. M. Vetrichelvan, L. Mihet-Popa, and J. B. Holm-Nielsen, ``A compre- hensive review on renewable energy development, challenges, and policies of leading Indian states with an international perspective,'' IEEE Access, vol. 8, pp. 74432_74457, 2020.

[3] S. Kumar, R. K. Saket, D. K. Dheer, J. B. Holm-Nielsen, and P. Sanjeevikumar, ``Reliability enhancement of electrical power sys- tem including impacts of renewable energy sources: A comprehensive review,'' IET Gener., Transmiss. Distrib., vol. 14, no. 10, pp. 1799_1815, May 2020.

[4] I. Masenge and F. Mwasilu, ``Hybrid solar PV-wind generation system coordination control and optimization of battery energy storage system for rural electri_cation,'' in Proc. IEEE PES/IAS PowerAfrica, Aug. 2020, pp. 1_5.

[5] N. Priyadarshi, S. Padmanaban, M. S. Bhaskar, F. Blaabjerg, and J. B. Holm-Nielsen, ``An improved hybrid PV-wind power system with MPPT for water pumping applications,'' Int. Trans. Electr. Energy Syst., vol. 30, no. 2, p. e12210, Feb. 2020.

[6] S. Padmanaban, K. Nithiyananthan, S. P. Karthikeyan, and J. B. Holm-Nielsen, Microgrids. Boca Raton, FL, USA: CRC Press, 2020.

[7] A. Suman, ``Role of renewable energy technologies in climate change adaptation and mitigation: A brief review from Nepal,'' Renew. Sustain. Energy Rev., vol. 151, Nov. 2021, Art. no. 111524. [Online]. Available:

https://www.sciencedirect.com/science/article/pii/S1364032121008029

[8] L. Varshney, A. S. S. Vardhan, S. Kumar, R. Saket, and P. Sanjeevikumar, ``Performance characteristics and reliability assessment of self-excited induction generator for wind power generation,'' IET, Renew. Power Gener., vol. 15, pp. 1927_1942, 2021.

[9] M. Seapan, Y. Hishikawa, M. Yoshita, and K. Okajima, ``Temperature and irradiance dependences of the current and voltage at maximum power of crystalline silicon PV devices,'' Sol. Energy, vol. 204, pp. 459_465, Jul. 2020. [Online]. Available: https://www.sciencedirect.com/science/article/pii/S0038092X20305089

[10] F. Mebrahtu, B. Khan, P. Sanjeevikumar, P. K. Maroti, Z. Leonowicz, O. P. Mahela, and H. H. Alhelou, ``Harmonics mitigation in industrial sector by using space vector PWM and shunt active power _lter,'' in Proc. IEEE Int. Conf. Environ. Electr. Eng., IEEE Ind. Commercial Power Syst. Eur. (EEEIC/I&CPS Europe), Jun. 2020, pp. 1_6.

[11] S. Vadi, S. Padmanaban, R. Bayindir, F. Blaabjerg, and L. Mihet-Popa, ``A review on optimization and control methods used to provide transient stability in microgrids,'' Energies, vol. 12, no. 18, p. 3582, Sep. 2019.

[12] N. Priyadarshi, S. Padmanaban, R. K. Ghadai, A. R. Panda, and R. Patel, ``Advances in power systems and energy management select proceedings of ETAEERE 2020,'' in Power System and Energy. Springer, 2020, p. 4.

[13] [13] E. Sundaram and M. Venugopal, ``On design and implementation of three phase three level shunt active power _lter for harmonic reduction using synchronous reference frame theory,'' Int. J. Electr. Power Energy Syst., vol. 81, pp. 40_47, Oct. 2016.

[14] A. Raj, S. R. Arya, and J. Gupta, ``Solar PV array-based DC_DC converter with MPPT for low power applications,'' Renew. Energy Focus, vol. 34, pp. 109_119, Sep. 2020. [Online]. Available: https://www.sciencedirect.com/science/article/pii/S1755008420300193

[15] C. H. Basha and C. Rani, ``Different conventional and soft computing MPPT techniques for solar PV systems with high step-up boost con- verters: A comprehensive analysis,'' Energies, vol. 13, no. 2, p. 371, Jan. 2020.

[16] J. D. Kumar, K. Mantosh, M. S. Bhaskar, P. Sanjeevikumar, J. B. H. Nielsen, and Z. Leonowicz, ``Investigation studies of DC_ DC boost converter with proportional-integral-derivative controller using optimization techniques,'' in Proc. IEEE Int. Conf. Environ. Electr. Eng., IEEE Ind. Commercial Power Syst. Eur. (EEEIC/I&CPS Europe), Jun. 2020, pp. 1_5.

[17] K. Gulyamov, R. Yunusov, S. Dovudov, B. Sharifov, A. Ghulomzoda, and M. Safaraliev, ``Increase in power of DC/DC converters with increased number of conversion channels,'' in Proc. Ural Smart Energy Conf. (USEC), Nov. 2020, pp. 59_62.

[18] N. Hawkins, B. Bhagwat, and M. L. McIntyre, ``Nonlinear current-mode control of SCIG wind turbines,'' Energies, vol. 14, no. 1, p. 55, Dec. 2020.

[19] A. M. M. dos Santos, L. T. P. Medeiros, L. P. S. Silva, I. D. S. Junior, V. S. de C. Teixeira, and A. B. Moreira, ``Wind power system connected to the grid from squirrel cage induction generator (SCIG),'' in Proc. IEEE 15th Brazilian Power Electron. Conf., 5th IEEE Southern Power Electron. Conf. (COBEP/SPEC), Dec. 2019, pp. 1_6.

[20] A. K. S. Tomar, K. K. Gautam, and A. Lodhi, ``Integration of SCIG wind energy conversion systems to the grid,'' Int. J. Eng. Sci. Invention, vol. 9, no. 6, pp. 28_36, 2020.

[21] B. B. Adetokun, C. M. Muriithi, and J. O. Ojo, ``Voltage stability analysis and improvement of power system with increased SCIG-based wind system integration,'' in Proc. IEEE PES/IAS PowerAfrica, Aug. 2020,pp. 1_5.

[22] M. Xu, L. Wu, H. Liu, and X. Wang, ``Multi-objective optimal scheduling strategy for wind power, PV and pumped storage plant in VSC-HVDC grid,'' J. Eng., vol. 2019, no. 16, pp. 3017_3021, Mar. 2019.

[23] P. Manoharan, U. Subramaniam, T. S. Babu, S. Padmanaban, J. B. Holm-Nielsen, M. Mitolo, and S. Ravichandran, ``Improved perturb and observation maximum power point tracking technique for solar photovoltaic power generation systems,'' IEEE Syst. J., vol. 15, no. 2, pp. 3024_3035, Jun. 2021.

[24] M. H. Reza and M. A. Shobug, ``Ef_ciency evaluation of P&O MPPT technique used for maximum power extraction from solar photovoltaic system,'' in Proc. IEEE Region Symp. (TENSYMP), Jun. 2020, pp. 1808_1811.

[25] A. Ali, K. Almutairi, S. Padmanaban, V. Tirth, and S. Algarni, ``Investigation of MPPT techniques under uniform and non-uniform solar irradiation condition_A retrospection,'' IEEE Access, vol. 8, pp. 127368_127392, 2020.